Assessment of mechanical, fracture and thermal properties of epoxy nanocomposites reinforced with low-concentration nano Boron Carbide (B_4C)

Akshata Ganji, Mantesh Choukimath
School of Mechanical Engineering, KLE Technological University, Hubballi, India
akshataganji91@gmail.com,
mantesh@kletech.ac.in, *https://orcid.org/0000-0001-7696-6037*

N.R. Banapurmath*
Centre of Excellence in Material Science, School of Mechanical Engineering, KLE Technological University, Hubballi-580031, India.
School of Mechanical Engineering, KLE Technological University, Hubballi-580031, India.
nr_banapurmath@kletech.ac.in, *https://orcid.org/0000-0002-1280-6234*

M. A. Umarfarooq*
Center for Material Science, Karpagam Academy of Higher Education, Coimbatore, Tamil Nadu 641 021, India.
Department of Mechanical Engineering Karpagam Academy of Higher Education, Coimbatore, Tamil Nadu 641 021, India.
umarfarooq.ma@gmail.com, *https://orcid.org/0000-0002-9369-7913*

Adavayya Chikkamath
School of Mechanical Engineering, KLE Technological University, Hubballi, India
chikkamathadavayya@gmail.com

Ashok M. Sajjan
Centre of Excellence in Material Science, School of Mechanical Engineering, KLE Technological University, Hubballi-580031, India.
am_sajjan@kletech.ac.in, https://orcid.org/0000-0003-1251-8803

Rajesh K.
Department of Robotics and Automation, Symbiosis Institute of Technology, Symbiosis International (Deemed University), Lavale, Pune-412115, Maharashtra, India,
rajeshkodbal@sitpune.edu.in

Ramesh M. Kenchappanavar
Department of Mechanical Engineering, Government polytechnic, Hubballi– 590018,
rameshmk88@gmail.com

Kartheek Ravulapati
Collins Aerospace, 5935, Pinnacle View Road, Cumming GA 30040, United States
kartheek.ravulapati@gmail.com

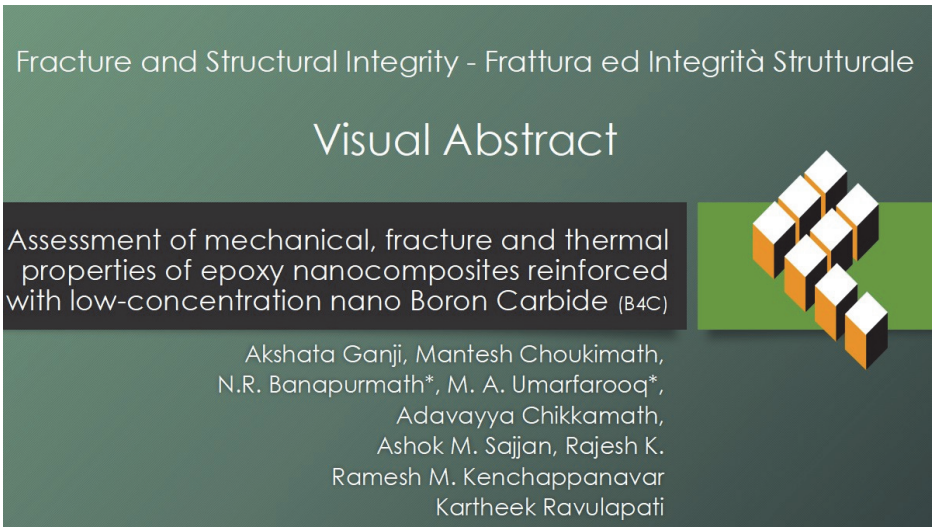

Citation: Ganji, A., Choukimath, M., Banapurmath, N.R., Umarfarooq M. A., Chikkamath, A., Sajjan, A. M., Rajesh, K., Kenchappanavar, R. M., Ravulapati, K., Assessment of mechanical, fracture and thermal properties of epoxy nanocomposites reinforced with low-concentration nano Boron Carbide (B_4C), Fracture and Structural Integrity, 74 (2025) 422-437.

Received: 15.07.2025
Accepted: 15.09.2025
Published: 21.09.2025
Issue: 10.2025

KEYWORDS. Boron carbide, Epoxy nanocomposites, Mechanical properties, Thermal properties, Fracture toughness, Finite element simulation.

INTRODUCTION

Epoxy resins are widely used in aerospace, automotive, domestic and civil structure applications due to their excellent adhesion, chemical and mechanical strength. However, their inherent brittleness and low fracture toughness limit their performance in high-demand applications. To overcome these limitations, researchers have explored incorporating nanomaterial reinforcements, such as organic, inorganic, ceramic and metal oxide nanoparticles [1 - 4]. One such promising material is B_4C, a lightweight ceramic known for its high hardness and thermal stability [5-6].

B_4C is one of the hardest materials with a Vickers hardness of approximately 30Hv, density of 2.52 g/cc, tensile modulus of 419.2±47.3 GPa, flexural strength of 585±70 MPa, and melting point of 2350 ºC [7-8]. Several studies have demonstrated that the incorporation of B_4C into epoxy resins improves mechanical and thermal performance. Kharat and Sidhu [9] investigated epoxy nanocomposites loaded with varying concentrations of B_4C and tungsten disulfide. The hardness and tensile strength increased with filler content, peaking at 2.5 wt.% B_4C and 4 wt. % tungsten disulfides. The maximum strength obtained was 32.69 MPa. Abenojar et al. [10] studied epoxy composites with micron-sized B_4C (7µm and 23µm). The addition of B_4C increased hardness and bending strength, with smaller particles demonstrating better performance due to improved dispersion and high surface area. Rallini et al. [11] reported that B_4C nanoparticles delayed thermal oxidation of carbon fibres in epoxy composites. The formation of boron oxide at high temperature acted as a protective layer, delaying further degradation. Also, cone calorimetry showed a 23% reduction in peak heat release rate with 5 wt. % filler. Galehdari and Kelkar [12] revealed that B_4C-epoxy composites maintained mechanical and thermophysical properties after exposure to neutron radiation, confirming their suitability for aerospace and nuclear environments.

While the previous studies on B_4C-epoxy composites focused on higher filler concentrations to enhance mechanical strength and thermal performance, the potential of low-concentration formulations remains unexplored. In this work, the effects of low concentration addition (0.1 – 0.4 wt. %) of nano B_4C on the mechanical, fracture and thermal properties are investigated. Epoxy nanocomposites loaded with B_4C at varying concentrations were prepared by solution casting techniques. The effects of filler addition were investigated through mechanical (tensile, flexural and impact) tests, thermal studies (DSC) and fracture tests. The fractured surfaces from the tensile tests were studied through SEM to understand the effect of filler addition on the fracture mechanism. Also, the experimental results were validated using the FE simulation of the tensile tests.

HIGHLIGHTS

This study demonstrates that low concentration loading (0.1 wt. % - 0.4 wt. %) of B_4C nanopowder significantly enhances the mechanical, thermal and fracture properties of epoxy nanocomposites. An improvement of up to 71% in tensile strength and 69.7% in fracture toughness was achieved. These enhancements are attributed to the effective nanoparticle dispersion and strong matrix-filler interaction, as confirmed by SEM analysis and thermal characterisation showing restricted polymer chain mobility and higher glass transition temperature. Finite element simulations further validated the experimental results, showing close agreement within 15%, while critically addressing the research gap in low-concentration B_4C-epoxy composites by creating a balance between performance and nanofiller content to reduce agglomeration effects.

EXPERIMENTAL DETAILS

Materials used

The base matrix material for this study was a two-part thermosetting part system. The resin used was a medium-viscosity unmodified Diglycidyl Ether of Bisphenol A type epoxy (Lapox L12), and the resin was cured with a polyamide-based hardener(K6). The polyproducts were sourced from C S Marketing, Bengaluru, India. The resin and hardener were mixed in a weight ratio of 9:1, as recommended by the manufacturer.

The nanoscale reinforcing filler used was boron carbide (B_4C) powder, procured from Nanoshel, Sundran, India. According to the technical data sheet of the supplier, the powder had an average particle size of less than 60 nm and a stated purity of 99.9%. The key properties of the nano-B_4C particles, as provided by the manufacturer and supported by the literature values for bulk B_4C material [7,8], are summarised in Tab. 1.

Density (in g/cc)	Tensile Modulus (GPa)	Poisson coefficient	Average particle size (nm)	Purity
2.25	472 [7]	0.18 [7]	< 60 nm	99.9%

Table 1: Properties of nano B_4C reinforcement particles.

Preparation of nanocomposites

The overall experimental methodology, from preparation to characterisation and simulation, is summarised in the flowchart presented in Fig. 1. The preparation process of epoxy-nanocomposites, as illustrated in Fig. 2, involves the following steps [13-14]. Initially, a 90 ml of epoxy resin is preheated at 50 ºC for 30 minutes to reduce its viscosity. A precise amount of B_4C (0.1 wt .% - 0.4 wt.%) nano powder is then added to the preheated resin, and the mixture is stirred using a mechanical stirrer for 30 minutes. Then, the mixture is subjected to an ultrasonication process for 45 minutes to ensure uniform dispersion of nanoparticles and reduce agglomeration. Following this, 10 ml of hardener is then added to the mixture and thoroughly mixed to initiate the curing process. The resulting solution is poured into the mould and allowed to cure at room temperature for 24 hours. After curing, the nanocomposites are cut into specimens as per ASTM standards for further testing. The configuration of the prepared nanocomposites is provided in Tab. 2.

Sl. No.	Specimen code	Matrix (wt. %)	B_4C (wt.%)
1	PE	100	-
2	EBC1	99.9	0.1
3	EBC2	99.8	0.2
4	EBC3	99.7	0.3
5	EBC4	99.6	0.4

Table 2: Configuration of Epoxy nanocomposite.

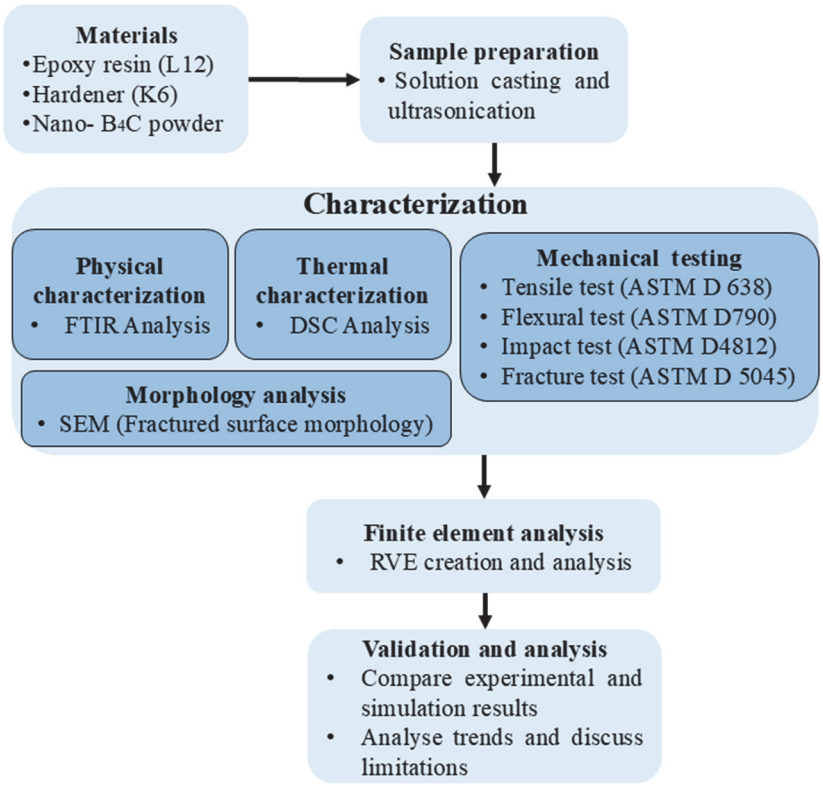

Figure 1: Flowchart of methodology.

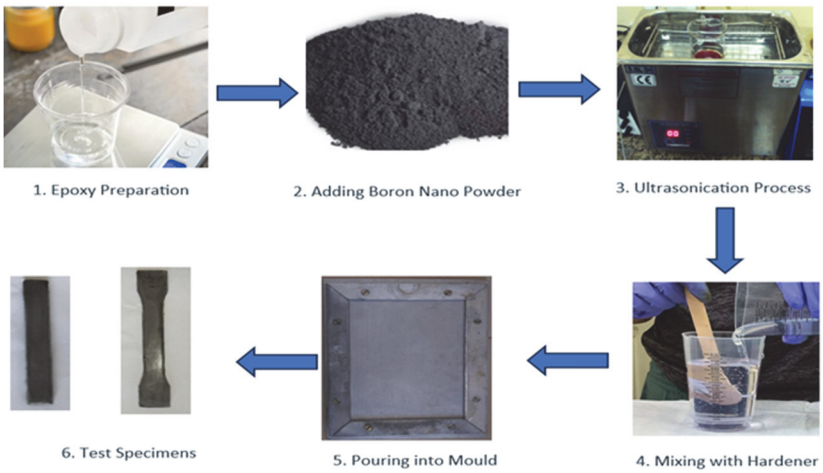

Figure 2: Steps for preparation of nanocomposites.

CHARACTERIZATIONS

A comprehensive set of characterisation techniques was used to evaluate the chemical, thermal, mechanical and fracture properties of prepared nanocomposites. The procedures for each analysis are provided in the subsequent section.

Fourier transform infrared (FTIR) analysis

FTIR analysis was performed to identify functional groups and investigate potential chemical interactions between the matrix and B_4C fillers. The analysis was conducted using a Perkin-Elmer System Series 2000 spectrophotometer. Small fragments of the composite sample were placed directly onto the attenuated total reflectance (ATR) crystal. Spectra were

recorded in the wavenumber range of 4000 to 500 cm^{-1} with 32 scans at 4 cm^{-1}. These recorded spectra were analysed with Lab Solution software®. The data obtained were plotted as a function of % transmittance vs wavenumber, cm^{-1}.

DSC analysis

The thermal behaviour, specifically the glass transition temperature (Tg), of the nanocomposites was studied using a differential scanning calorimeter (Shimadzu DSC 60 Plus, Tokyo, Japan). For each test, a sample of weight 4–5 mg was accurately weighed using a microbalance and sealed in an aluminium pan and crimped systematically. An empty aluminium crucible was used as a reference. The samples were heated over a temperature range of 30–350 ◦C at a heating rate of 10 ◦C/min, the purge gas nitrogen was allowed to flow at the rate of 100 ml/min and the thermograms obtained were analysed using the software Lab Solutions®.

Tensile tests

Tensile properties were determined according to ASTM D638[15] using Type-I specimens. The tests were carried out on a Tinius Olsen UTM with 10 kN capacity. The specimens were gripped firmly, and a constant crosshead displacement rate of 3 mm/min was applied until failure. The tensile strength and modulus were calculated automatically by the machine's software from the resulting stress-strain curves. The dimensions of the specimen used are shown in Fig. 3.

Flexural tests

Three-point flexural tests were conducted as per ASTM D790 [16]. Rectangular bar specimens were placed on two supports with a span length of 48 mm (maintaining a 16:1span to depth ratio). A loading nose was applied at the mid-span at a constant crosshead speed of 1 mm/min until rupture. The dimensions of the specimen used are shown in Fig. 3. The flexural strength was calculated using Eqn. (1).

$$\sigma_f = \frac{3PL}{2hd^2} \tag{1}$$

where, σ_f - flexural strength, P – Peak load, L – span length, b – width of specimen, d- depth of specimen.

Impact test

Unnotched Izod impact strength was measured as per ASTM D4812 [17] using a Zwick/Roell Hit 50P pendulum impact tester. The specimens, with dimensions shown in Fig.3, are clamped into the pendulum impact test fixture with the thin edge facing the striking edge of the pendulum. The pendulum is released and allowed to strike through the specimen. The energy absorbed during the fracture is recorded, and the impact strength is calculated.

Fracture tests

The fracture toughness was evaluated using single-edged notched beam (SENB) test specimens as per ASTM D5045 [18]. A sharp pre-crack was introduced at the tip of the machined notch in the specimen by tapping a fresh razor blade. The pre-cracked specimen (Fig. 3) was then loaded in a three-point bending fixture on a Tinius Olsen UTM (10 kN capacity) with a support span of 48 mm and a very slow cross speed of 0.5 mm/min. to ensure stable crack growth. The span length maintained was four times the width of the specimens, and the displacement rate used was. The fracture toughness (K_{IC}) was calculated by Eqn.(2):

$$K_{IC} = \left(\frac{P_Q}{B\sqrt{W}} \right) f(x) \tag{2}$$

where $0.2 < x < 0.8$

$$f(x) = 6x^{0.5} \frac{\left[1.99 - x(1-x)\left(2.15 - 3.93x + 2.7x^2\right) \right]}{(1+2x)(1-x)^{1.5}}$$

where P_Q – Load (kN); B- thickness of specimen (cm); W- width of specimen (cm); a - crack length in cm, and x = a/w

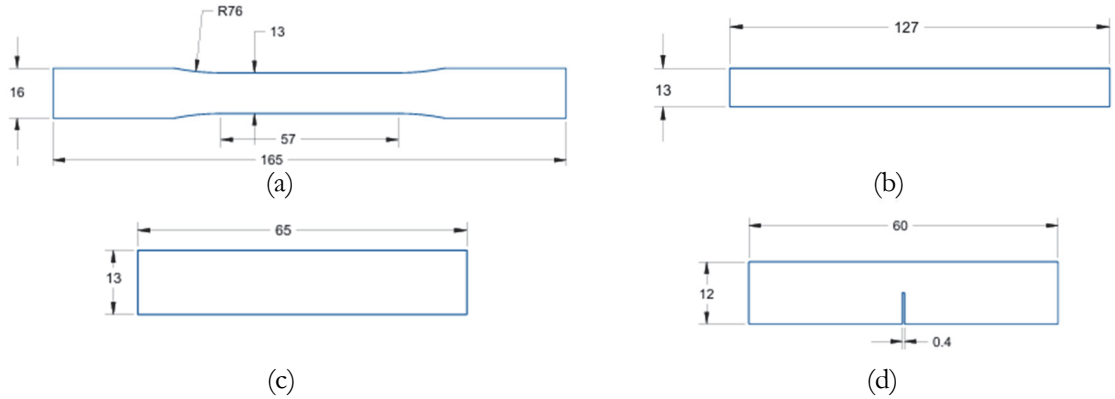

Figure 3: Dimensions of specimens for (a) Tensile (b) Flexural (c) Impact (d) Fracture tests

RESULTS AND DISCUSSIONS

FTIR analysis

The FTIR spectra of neat epoxy and nanocomposites with varying concentrations of B_4C, shown in Fig. 4, provide valuable insights into chemical interactions between the epoxy matrix and B_4C fillers. The spectrum for PE displays characteristic peaks, including O-H stretching vibration around 3408 cm^{-1}, distinct C-H stretching peaks between 2800-3000 cm^{-1}, aromatic C=C vibrations at 1508 cm^{-1}, strong C-O-C ether linkage absorptions at 1243 cm^{-1} and the characteristic epoxy ring vibration at 915 cm^{-1} [19-20]. With the addition of B_4C, subtle changes are observed in the spectra, particularly in EBC1, where minor shifts and changes in peak intensities indicate weak interactions between the filler and the matrix. As the filler concentration increases in EBC2, EBC3 and EBC4, the spectra exhibit broader O-H peaks around 3500 cm^{-1} and enhanced absorption in the 600 – 1500 cm^{-1} region, implying stronger interactions between epoxy and B_4C. Also, a decrease in transmittance with the increasing filler content highlights higher absorption and improved filler-matrix compatibility.

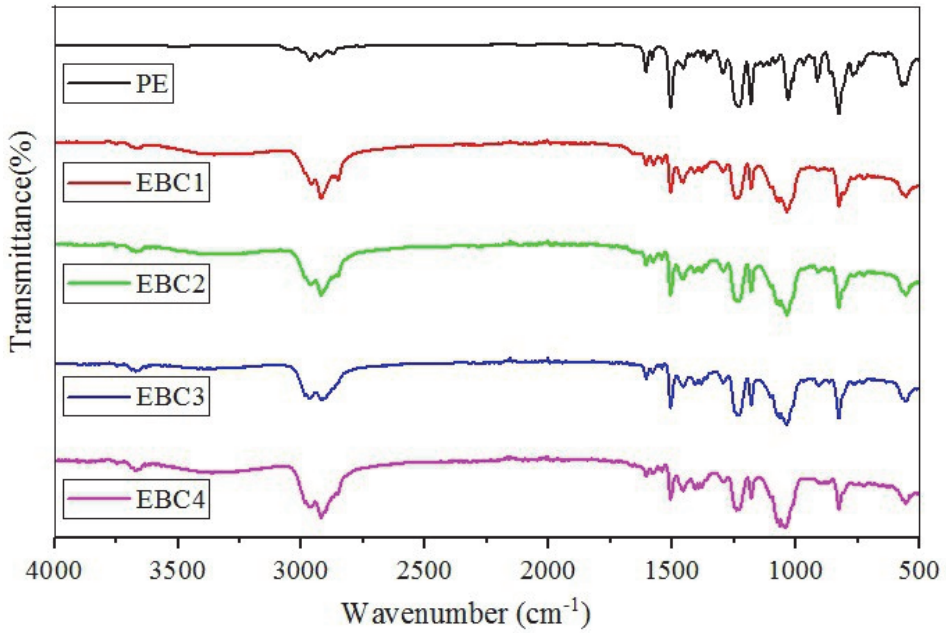

Figure 4: FTIR spectrum of PE and their nanocomposites.

DSC analysis

The DSC analysis of the PE and nanocomposites, as shown in Fig. 5, demonstrated a distinct thermal behaviour due to the incorporation of filler. Pure epoxy exhibits a Tg at 52.49°C, followed by an exothermic curing peak at 63°C and a sharp degradation phase. Upon addition of B_4C, the nanocomposites exhibit a sharp increase in Tg with EBC1at 64.09°C, EBC2 at 65.04 °C, EBC3 at 65.96°C, and EBC4 at 68.02 °C, indicating a polymer restricted mobility. The heat flow profiles also indicate a notable trend of reduced enthalpy of transitions with increasing B_4C content in the epoxy composites. This reduction can be attributed to the restricted molecular mobility within the epoxy matrix, which arises from the incorporation of the B_4C nanoparticles. As the B_4C content increases, the heat flow peaks become less noticeable, likely due to restricted molecular mobility within the composites. These results highlight the role of B_4C in enhancing the thermal performance and stability of the epoxy composites.

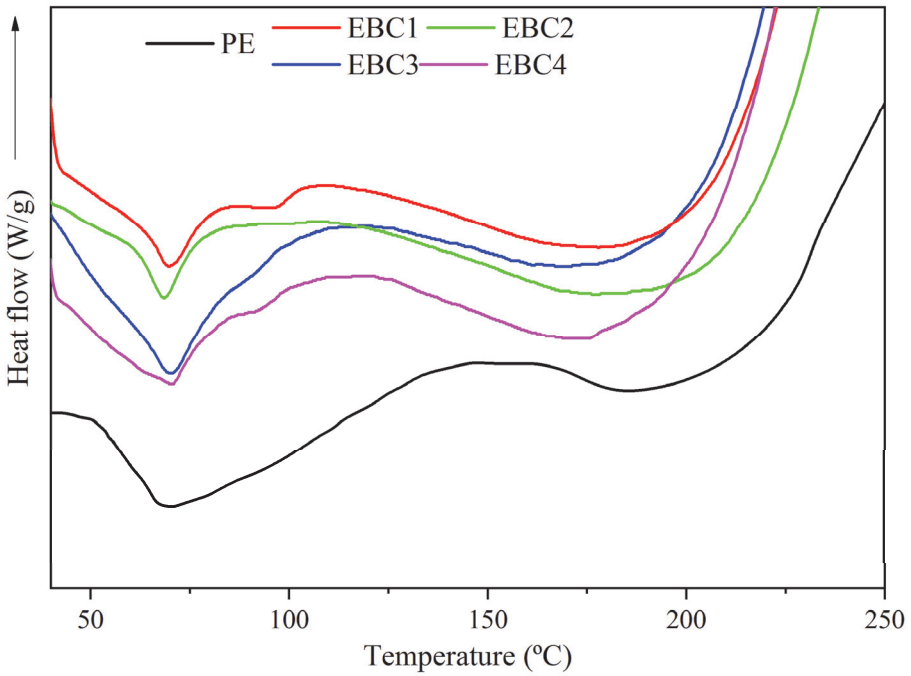

Figure 5: DSC curves of PE and its nanocomposites.

Tensile tests

The tensile strength and modulus of the neat epoxy and B_4C-loaded nanocomposites are shown in Fig. 6 and Fig. 7, respectively. The nanocomposites demonstrate significant improvement in tensile properties with increasing B_4C content. The tensile strength increased from 18.17 MPa (PE) to a peak of 31.2 MPa (EBC3), exhibiting a 71% improvement and a reduction to 25.8 MPa (EBC4), likely due to the agglomeration of nanoparticles at higher concentration, as shown in Fig. 8(e). However, the tensile modulus showed a consistent increase from 1050 MPa (PE) to 1400 MPa (EBC4), exhibiting a 33% increase in the modulus.

The enhancement in tensile strength and modulus can be explained through efficient stress transfer at the nanoparticle-matrix interface. B_4C nanoparticles, with their exceptionally high modulus (472 GPa) and hardness (30 HV), act as rigid reinforcements that bear a significant portion of the applied load, reducing strain in the surrounding matrix. At low concentrations (0.1 – 0.4 wt.%), the high aspect ratio and surface area of B_4C particles promote strong van der Waals and possible covalent interactions with the epoxy chains, as demonstrated by FTIR shifts in the 600 – 1500 cm^{-1} region (Fig. 4), indicating improved interfacial adhesion. This adhesion facilitates load transfer, delaying matrix yielding and crack initiation. The peak strength at 0.3 wt.% reflects optimal dispersion, where nanoparticles create a percolated network that homogenises stress distribution. Beyond this, agglomeration – driven by interparticle van der Waals forces – creates stress concentrations, acting as flaw sites that lower the effective reinforcement efficiency and reduce strength by 17% from the peak. This is consistent with percolation theory in nanocomposites, where filler clustering shifts the system from reinforcement to defect-dominated behaviour. The steady modulus increase, however, is less sensitive to agglomeration because it primarily depends on the volume fraction and intrinsic stiffness of B_4C, following the rule-of-mixture models modified for nanoscale effects (Hashin-Tsai equation), where even clustered particles contribute to overall rigidity.

The increase in tensile strength and modulus aligns with prior studies on B_4C-epoxy composites [9-12], where the nanoparticle dispersion and interfacial adhesion were critical. The reduction in the tensile strength at 0.4 wt% B_4C correlates with the SEM evidence from the prior studies. Choukimath et al. [21] demonstrated that graphene nanoplatelets loaded epoxy composites with 0.3 wt. % fillers exhibited uniform dispersion, while 0.4 wt. % showed agglomerates, reducing strength by 18%. Similarly, Nimbagal et al. [22] attributed strength loss at high carbon nano-fibre concentrations to voids and poor interfacial adhesion. The steady rise in the modulus with B_4C content reflects efficient stress transfer, similar to graphene reinforced epoxy composites as reported by Dileep et al. [14,19], where a 46% increase in modulus with 0.1 wt. % GNPs due to their high specific area and strong matrix adhesion. Recent work on boron-doped epoxy composites further supports the efficacy of low-concentration boron-based fillers in improving mechanical properties. Hiremath et al. [23] demonstrated that the epoxy composite with 0.3 wt.% boron nanoparticles exhibited optimal tensile strength (16.8 MPa) attributed to uniform dispersion and effective stress transfer. Beyond 0.3 wt. % agglomeration effects reduced performance, a trend consistent with observations in B_4C reinforced composites.

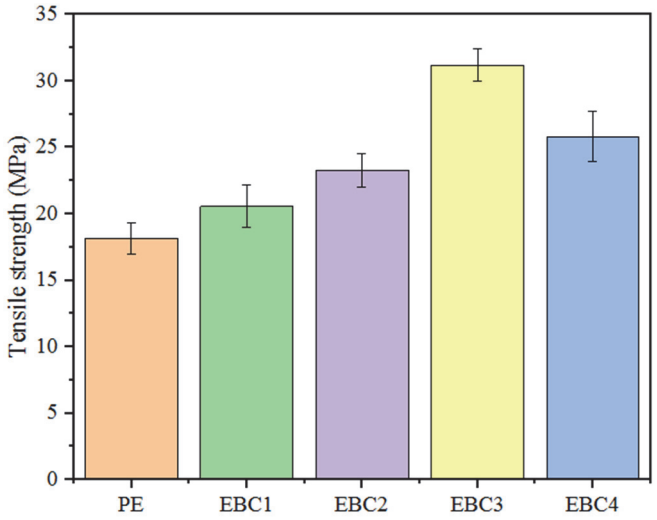

Figure 6: Tensile strength of all composite samples.

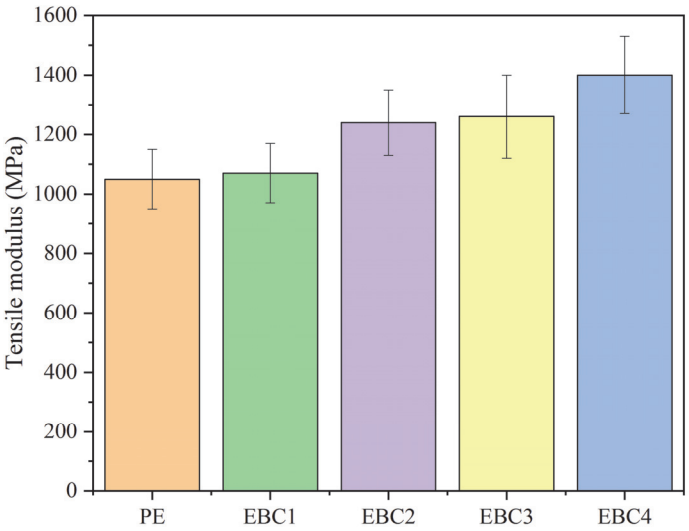

Figure 7: Tensile modulus of all composite samples.

SEM imaging of the fractured surface from tensile tests was conducted to evaluate the morphology, filler distribution, and matrix-filler interactions in the B_4C reinforced epoxy composites [22,23]. The micrographs reveal distinct differences in fracture behaviour with increasing B_4C content. The neat epoxy (PE, Fig. 8(a)) exhibits a smooth fracture surface, characteristic of brittle fracture, with no visible voids or defects, indicating rapid crack propagation and low energy

absorption, consistent with its low tensile strength (18.17 MPa) and fracture toughness (1.75 MPa.m$^{0.5}$). In contrast, the B4C-loaded composites (EBC1 – EBC4, Fig. 8 b-e) display increasingly complex morphologies due to nanoparticle reinforcement. For EBC1 (Fig. 8(b)), the fracture surface shows slight roughening. This indicates initial crack deflection, contributing to a slight tensile strength increase (19.73 MPa, 8.5 % improvement). EBC exhibits a moderately rougher surface with clearly visible cleavage planes, demonstrating enhanced crack pinning and energy dissipation, correlating with a 25 % increase in tensile strength (22.70 MPa). The EBC3 composite, which exhibited the highest tensile strength (31.2 MPa, 71% improvement), displays the roughest and most torturous fracture surface, dominated by a high density of fine, stepped cleavage planes. This complex topography signifies effective crack pinning and deflection, increasing the fracture area and energy dissipation. Furthermore, the strong interfacial adhesion, inferred from the restricted polymer chain mobility in DSC results, enables effective stress transfer from the softer epoxy to rigid B_4C particles (472 GPa modulus). Conversely, EBC4 shows a rough but less effective fracture surface, with larger and coarser cleavage planes and evidence of nanoparticle agglomeration. These clusters act as stress concentration sites, initiating microcracks and causing a 17% drop in tensile strength (25.8 MPa) compared to EBC3.

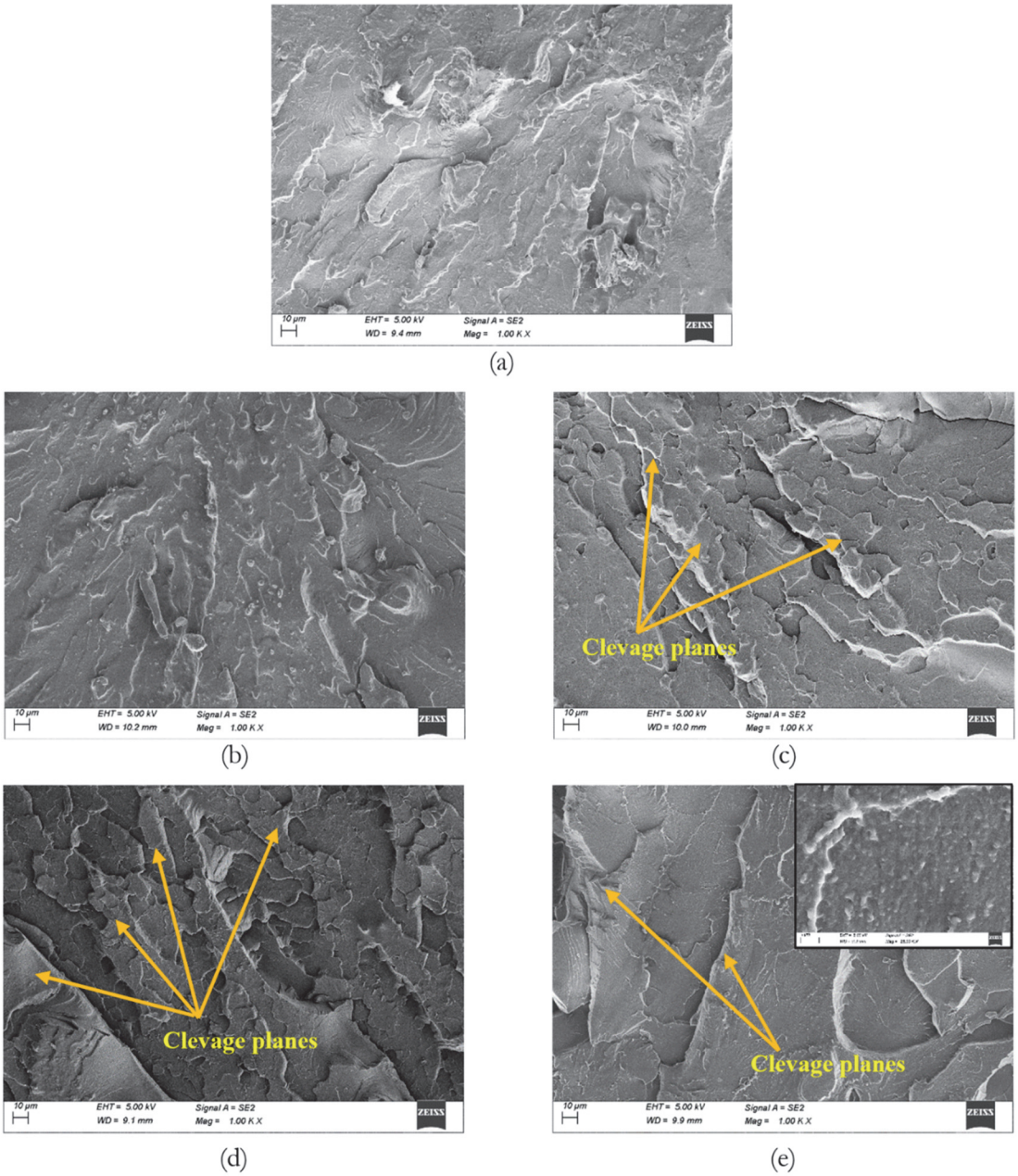

(a) (b) (c) (d) (e)

Figure 8: SEM images of (a) PE, (b) EBC1, (c) EBC2, (d) EBC3, and (e) EBC4

Microstructural and compositional analysis

Energy-dispersive X-ray (EDAX) spectroscopy was performed on the fractured surface of neat epoxy and B_4C-reinforced nanocomposites to verify the presence of the B_4C fillers. Fig. 9 presents the EDAX spectra of all samples. The neat epoxy (Fig. 9(a)) displayed only carbon (C) and oxygen (O) peaks, characteristic of an organic polymer matrix, with no detectable boron (B) signal. In contrast, the spectra of B_4C-loaded nanocomposites (Fig. 9(b-e)) exhibited a distinct boron peak. This confirmed the incorporation of B_4C nanoparticles into the epoxy matrix. The high carbon content originates from the epoxy matrix, while the simultaneous presence of boron and carbon peaks in the nanocomposites provides conclusive evidence of the compositional modification achieved through reinforcement. These EDAX findings, together with SEM fractographs (Fig. 8), confirm that B_4C nanoparticles were not only incorporated but also contributed to microstructural modification in the epoxy.

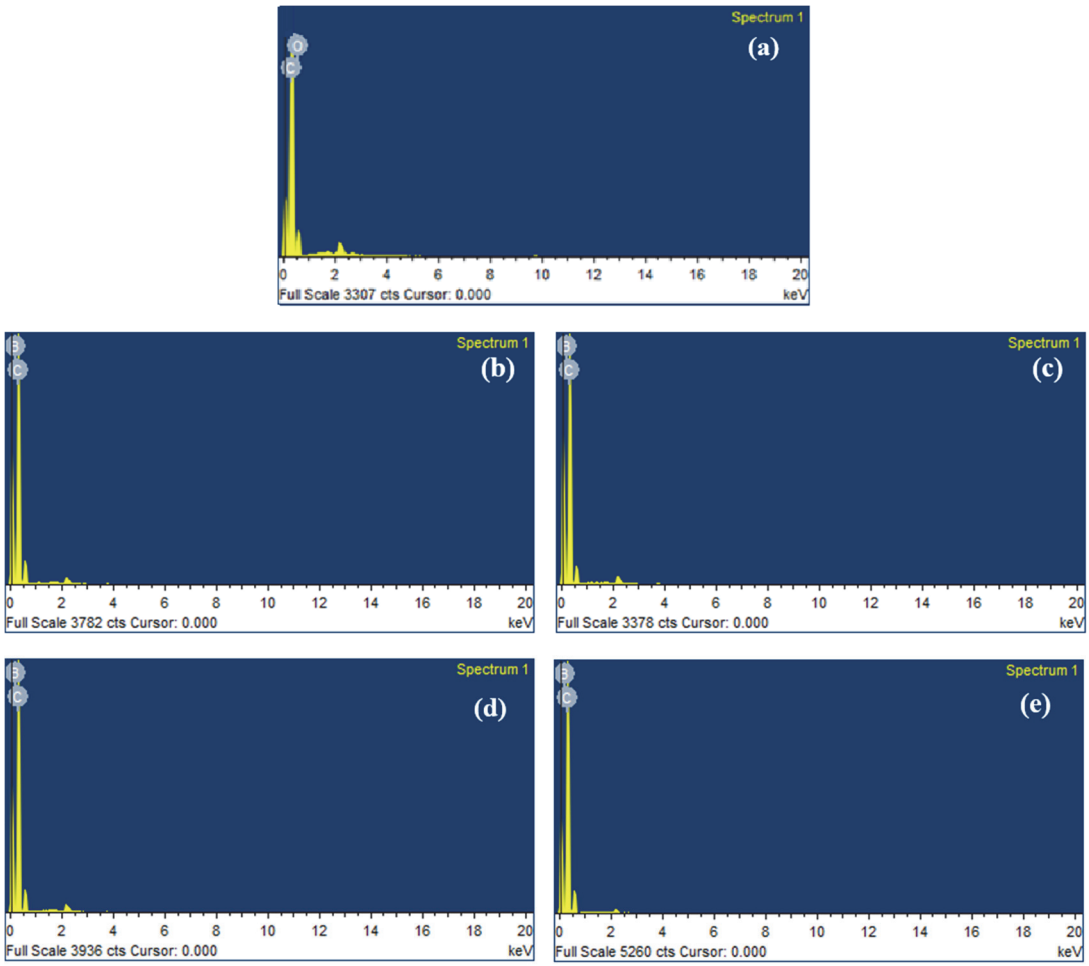

Figure 9: EDAX spectrum of (a) PE, (b) EBC1, (c) EBC2, (d) EBC3, and (e) EBC4.

Flexural tests

The flexural strengths evaluated from the 3-point bending tests are provided in Fig. 10. The flexural strength demonstrated a progressive increase with higher B_4C content, with neat epoxy exhibiting 47.21 MPa, while B_4C composites showed 15.4% (54.46 MPa for EBC1), 20.5 % (58.95 MPa for EBC2), 36.2% (64.31 MPa for EBC3), and 49.3 % (70.46 MPa for EBC4) improvements, respectively.

Unlike tensile loading, where uniform uniaxial stress predominates, flexural stress involves compressive and tensile gradients across the specimen thickness, making them sensitive to surface and interfacial effects. B_4C particles bridge microcracks, distributing shear stresses more evenly and preventing delamination. The progressive improvement in strength suggests that agglomeration effects are mitigated under bending, possibly because localised compressive zones suppress cluster-induced flaws. This aligns with the higher surface area of B_4C nanoparticles, facilitating better wetting and adhesion and enhancing flexural strength through increased cross-link density, as hinted by DSC's restricted chain mobility (Fig. 5). The progressive

improvement in flexural strength with B_4C loading contrasts with typical nanoparticle reinforced epoxies [19,21], where agglomeration beyond 0.3 wt. % often reduces performance. The results align with Xie et al.,[24] who reported a 20% increase in flexural strength with just 0.5 vol.% cellulose nanofibers in epoxy.

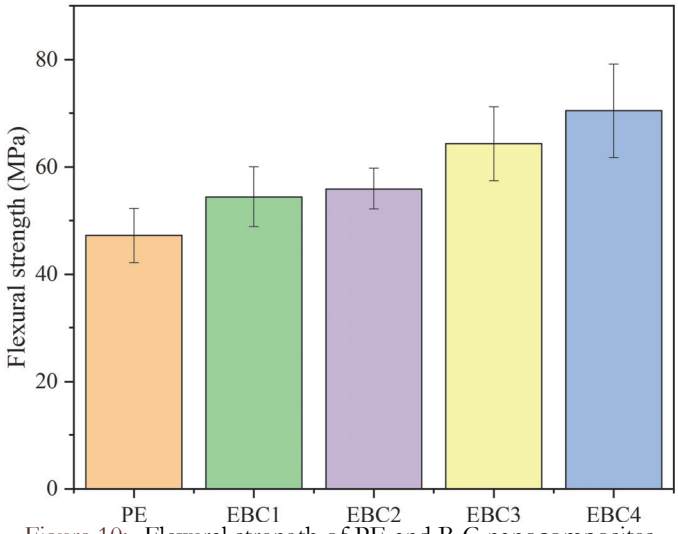

Figure 10: Flexural strength of PE and B_4C nanocomposites.

Impact tests

The impact strength results shown in Fig. 11 demonstrate significant improvement with B_4C reinforcement, increasing from 25.66 J/m for neat epoxy to 41.56 J/m for EBC4, demonstrating a 62% enhancement. While lower B_4C loadings resulted in relatively smaller improvements, with EBC1 showing only 2% increase (26.15 J/m) compared to pristine epoxy, the impact strength enhancements in the higher loadings were much higher. EBC2, EBC3, and EBC4 composites exhibited substantial improvements of 16%, 37%, and 62% respectively.

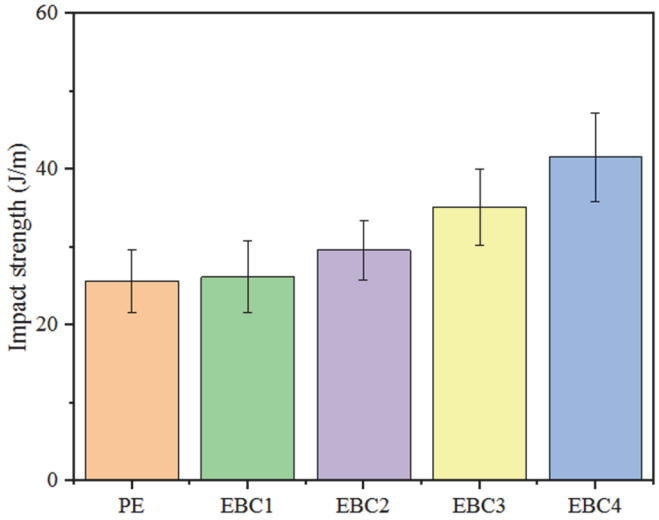

Figure 11: Impact strength of PE and B_4C nanocomposites.

The addition of B_4C nanoparticles improves impact resistance by creating pathways for energy absorption, primarily through debonding from the matrix and the formation of plastic zones around them. Their high thermal conductivity aids in dissipating localised heat from rapid deformation, preventing thermal softening of the matrix. At higher concentrations, the nanoparticles form a network that promotes distributed microcracking over a single dominant crack, increasing toughness via extrinsic mechanisms like crack bridging. This is supported by rougher SEM fractographs (Fig. 8), which show that increased surface area correlates with higher energy absorption. This higher performance of the nanocomposites demonstrates the effectiveness of B_4C in toughening the epoxy matrix, likely through the crack deflection and energy

absorption mechanisms as observed in SEM analysis [Fig. 8] of fractured surfaces. In a study by Nimbagal et al. [22] on epoxy-polylactic acid nanocomposites, the impact strength showed a consistent rise with increasing CNF content up to 0.3 wt. %. However, at 0.4 wt. %, a reduction was observed, which was attributed to the agglomeration of the nanoparticles.

Fracture toughness

The fracture toughness of the pristine epoxy and B4C-loaded nanocomposites is shown in Fig. 12. The fracture toughness results demonstrate significant enhancement with the B_4C reinforcement, exhibiting a concentration-dependent pattern. PE exhibited a fracture toughness of 1.75 MPa.m$^{1/2}$, while B_4C reinforced composites exhibit progressive increases. EBC1, EBC2, EBC3 and EBC4 showed an enhancement by 9% (1.95 MPa.m$^{1/2}$), 22.9 % (2.15 MPa.m$^{1/2}$), 41.1% (2.47 MPa.m$^{1/2}$) and 69.7% (2.97 MPa.m$^{1/2}$), respectively. This steady improvement across all concentrations implies B_4C's effectiveness in toughening epoxy matrices.

The fracture toughness enhancement in B_4C reinforced nanocomposites is attributed to the creation of tortuous crack paths, as confirmed by the SEM images (Fig. 8). At the nanoscale, B_4C particles interact with advancing cracks via pinning (where particles anchor the crack front) and deflection (altering crack path trajectory to non-planar paths). This is rooted in the mismatch in elastic moduli between B_4C and epoxy matrix, generating local stress fields that bend the cracks around particles. Strong interfacial bonding, evidenced by FTIR (Fig. 4), prevents pull-out and promotes shear yielding in the matrix, contributing to intrinsic toughening.

Similar mechanisms have been observed in epoxy nanocomposites reinforced with GNPs and h-BNs [21], where improved interfacial bonding led to significant toughness improvement. The 69.7% enhancement in fracture toughness with 0.2 wt.% B_4C is comparable to the 49.25% improvement observed in h-BN reinforced epoxy composites at similar concentrations. The progressive enhancement in fracture toughness is governed by several micromechanical mechanisms. The hard B_4C particles act as obstacles, pinning the crack front and forcing it to change direction, thereby increasing the crack length and energy required for propagation. Subsequently, cracks are deflected around the particles, changing local crack growth direction. The rougher surfaces observed in SEM (Fig. 8) are a direct indication of a tortuous path.

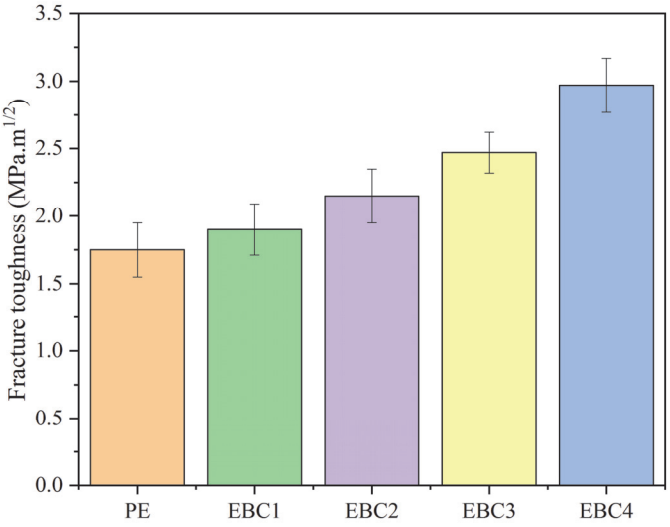

Figure 12: Fracture toughness of PE and B_4C nanocomposites.

SIMULATION STUDIES OF NANOCOMPOSITES

Numerical simulation using finite element (FE) simulation was carried out to predict the mechanical properties of the composites, with the computation results subsequently validated against the experimental data

Development of Representative Volume Element (RVE)

A three-dimensional microscale RVE of the nanocomposite was developed in the Material Designer module of ANSYS Workbench, as shown in Fig. 13. The RVE was created by inputting the material properties of both constituent phases

(epoxy matrix and B_4C reinforcement particles) along with their respective weight fractions. After meshing the RVE geometry, periodic boundary conditions were applied to simulate the material's infinite periodic microstructure. The homogenised elastic properties of the nanocomposites were then computationally obtained, and these nanocomposite properties are used as input for simulation in static analysis of tensile and flexural specimens.

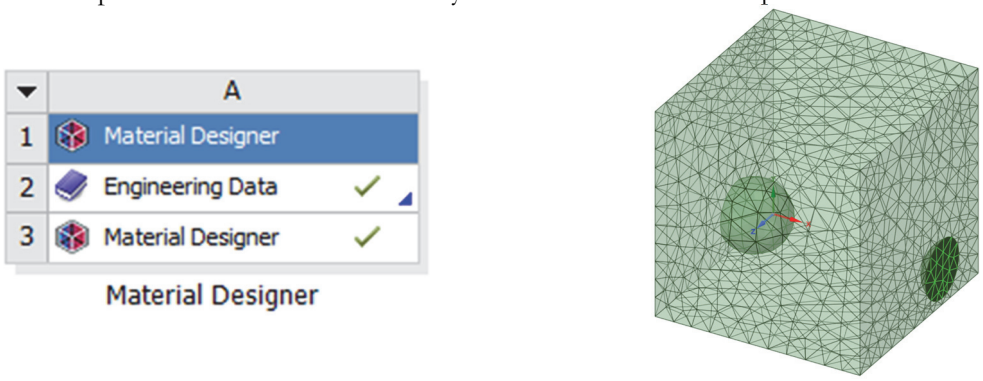

Figure 13: Images of the material designer module and RVE.

While the RVE approach provides a powerful tool for predicting homogenised elastic properties, its limitations must be acknowledged. The model assumes an idealised microstructure with perfectly dispersed, spherical particles and a perfectly bonded interface, which does not account for the agglomeration observed at higher filler loadings or the complex interfacial mechanisms that occur during fracture. Furthermore, the model predicts linear elastic behaviour and cannot capture the nonlinear damage progression and ultimate failure of the composites, potentially leading to an overestimation of strength.

Model creation and boundary conditions

Three-dimensional models of the tensile and bending specimens for FE simulation were created in SolidWorks, using the dimensions as specified in ASTM D638 and ASTM D790, respectively. The model was imported into the Static structural module of ANSYS Workbench. After meshing using Hex20 elements, the boundary conditions were applied. The boundary conditions used for tensile test and flexural test simulation are shown in Fig. 14. For tensile tests, one end of the specimen is clamped completely and a load is applied on the other end, whereas, for flexural test simulation, the specimen is loaded at the centre and supported at the two free ends. The simulation was carried out with boundary conditions similar to those of the experimental results. Maximum force values sustained by the specimen before failure were used as a benchmark for the simulation approaches.

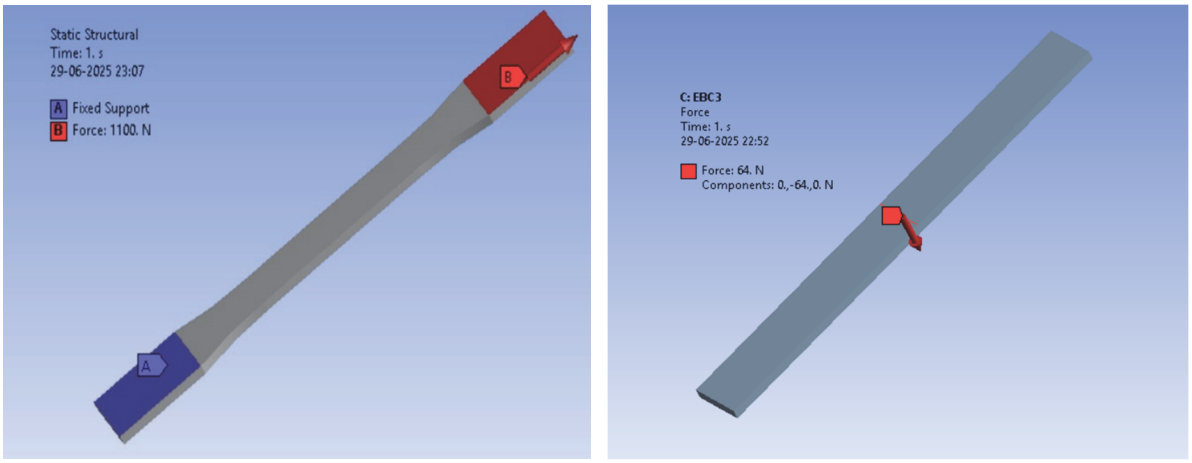

(a) (b)

Figure 14: Boundary conditions during simulation of (a) Tensile test, (b) Flexural test.

For an axial force of around 1100 N on the tensile specimen for EBC3, the equivalent von Mises stress developed as shown in Fig. 15(a) is very close to experimental data, according to the plots of the physical test (Fig. 6). On the other hand, a similar approach was used for simulating a 3-point flexural test, with simple support at two ends and force on the centre of

the specimen. For the EBC3 specimen, a load of 64 N was applied vertically downwards at the centre, and the variation of equivalent stress is shown in Fig. 15(b). Tab. 3 provides a comparison of tensile and flexural strengths of all specimens obtained from experimentation and FE Simulation. The variations in the tensile and flexural strength obtained from the experimentation and simulation were within 15%.

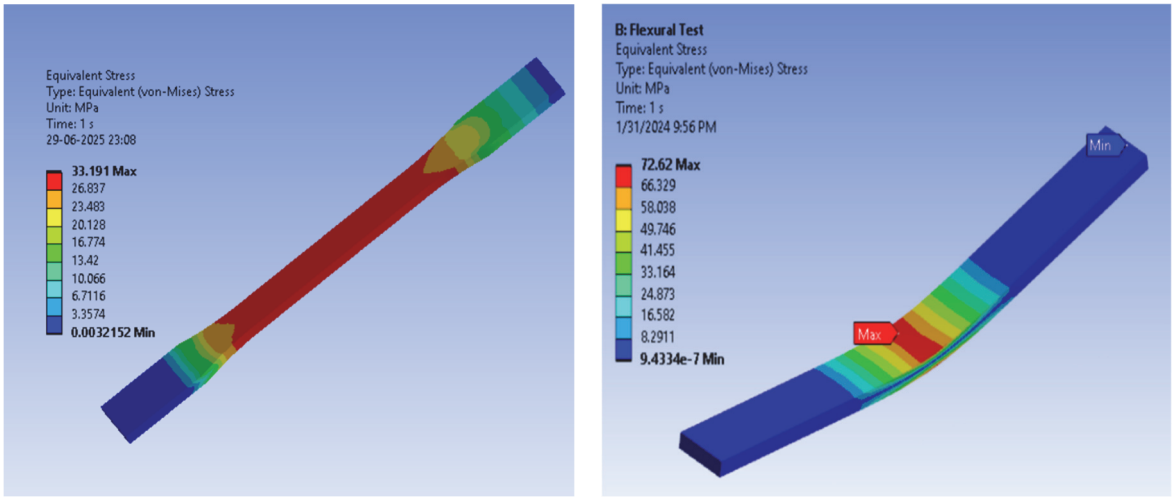

(a) (b)

Figure 15: Maximum equivalent stress from simulation of (a)Tensile test (b) Flexural test.

Nanocomposites	Tensile strength from FE simulation in MPa	Tensile strength from experimental results in MPa	Variation in results (in %)	Flexural strength from FE simulation in MPa	Flexural strength from experimental results in MPa	Variation in results (in %)
PE	19.09	18.17	5.05	49.52	47.21	4.89
EBC1	20.57	19.73	4.08	54.46	58.19	6.85
EBC2	23.27	22.70	2.45	55.95	60.41	7.97
EBC3	31.20	30.43	2.47	64.31	72.62	12.92
EBC4	25.80	24.17	6.32	70.46	79.50	12.83

Table 3: Comparison of tensile and flexural strengths obtained from experimentation and FE simulation.

STATISTICAL ANALYSIS

In statistical analysis, t-tests are used to determine whether there is a significant difference between the means of two groups. A series of independent two-sample t-tests was conducted to statistically evaluate the significance of the enhancements in tensile strength and fracture toughness resulting from the incorporation of nano-B4C fillers. A pure epoxy sample was used as the control group against each nanocomposite configuration (EBC1, EBC2, EBC3 and EBC4). The tests were performed at a significance level of $\alpha = 0.05$. The results are summarised in Tab. 4.

Comparison	Tensile strength		Fracture toughness	
	t-statistics	p-value	t-statistics	p-value
PE vs EBC1	5.18	0.0034	5.00	0.0038
PE vs EBC2	15.60	< 0.001	9.00	0.0003
PE vs EBC3	26.92	< 0.001	19.80	< 0.001
PE vs EBC4	19.48	< 0.001	24.93	< 0.001

Table 4: Statistical analysis of tensile strength and fracture toughness enhancements.

The results provided in Tab. 4 shows that all p-values for both tensile strength and fracture toughness are far below the 0.05 threshold. This confirms that the property improvements achieved even with the lowest concentration of nano-B_4C (0.1 wt.%) are statistically significant. The increase in the t-statistic values with higher filler concentrations provides strong statistical evidence for concentration-dependent efficiency of the B4C reinforcement, directly supporting the experimental trends observed in Fig. 6 and Fig. 12.

CONCLUSIONS

The study demonstrated that the incorporation of low concentration (0.1-0.4 wt.%) of nano-boron carbide (B_4C) significantly enhances the mechanical, thermal and fracture properties of epoxy nanocomposites. Tensile strength peaked at 0.3wt.% B_4C, demonstrating 71% enhancement (31.2 MPa) compared to neat epoxy, while the tensile modulus showed a steady increase, exhibiting 1400 MPa (33% improvement) at 0.4 wt.% due to the high stiffness of B_4C particles. Flexural strength exhibited a progressive rise with increasing B_4C content, showing a 49.3% improvement (70.46 MPa) at 0.4 wt. %, indicating effective resistance to bending stresses. Impact strength surged by 62% at the 0.4 wt. % B_4C, showing the filler role in toughening the epoxy matrix. Fracture toughness also improved steadily, with a 69.7% increase at 0.4 wt. %, attributed to the crack deflection and energy absorption mechanism. Thermal analysis revealed a higher glass transition temperature and improved stability due to the B_4C addition. SEM images confirmed enhanced fracture resistance, with rougher surfaces and finer cleavage planes in nanocomposites. Finite element simulations validated the experimental results, showing close agreement with the variations within 15%. Statistical analysis confirmed that these improvements were significant ($p < 0.05$). Overall, this study underlines the potential of low-concentration B_4C reinforcement to optimise the performance of the epoxy.

However, the solution casting and ultrasonication, while effective, may lead to nanoparticle clustering at higher concentrations, which impacts reproducibility and mechanical performance. Environmental factors such as humidity, ageing, and long-term thermal cycling were not studied, but could influence the durability and stability of the composites. The RVE-based simulations, though useful to predict homogenised elastic properties, tend to oversimplify interfacial interactions and fail to capture complex non-linear failure mechanisms.

The developed boron-carbon-based epoxy nanocomposites can be applied for lightweight aerospace and automotive components, electronic encapsulation, as well as for neutron shielding applications due to their enhanced toughness, thermal stability and boron's inherent protective properties. Future research will focus on optimising dispersing techniques to minimise agglomerations, studying the long-term performance under environmental exposure, and incorporating advanced multiscale modelling approaches to better capture fracture and damage mechanisms.

REFERENCES

[1] Jin, F.-L., Li, X., Park, S.-J. (2015). Synthesis and application of epoxy resins: A review, Journal of Industrial and Engineering Chemistry, 29, pp. 1–11. DOI: https://doi.org/10.1016/j.jiec.2015.03.026.

[2] Mohan, P. (2013). A Critical Review: The Modification, Properties, and Applications of Epoxy Resins, Polymer-Plastics Technology and Engineering, 52(2), pp. 107–125. DOI: https://doi.org/10.1080/03602559.2012.727057.

[3] Umarfarooq, M.A., Gouda, P.S.S., Nandibewoor, A., Banapurmath, N.R., Kumar, G.B.V. (2019). Determination of residual stresses in GFRP composite using incremental slitting method by the aid of strain gauge., Surathkal, India, p. 020038. DOI: https://doi.org/10.1063/1.5085609

[4] Sukanto, H., Raharjo, W.W., Ariawan, D., Triyono, J., Kaavesina, M. (2021). Epoxy resins thermosetting for mechanical engineering, Open Engineering, 11(1), pp. 797–814. DOI: https://doi.org/10.1515/eng-2021-0078.

[5] Suri, A.K., Subramanian, C., Sonber, J.K., Murthy, T.S.R.C. (2010). Synthesis and consolidation of boron carbide: a review, International Materials Reviews, 55(1), pp. 4–40. DOI: https://doi.org/10.1179/095066009X12506721665211.

[6] Zhang, W. (2023). Recent progress in B4 C–SiC composite ceramics: processing, microstructure, and mechanical properties, Mater. Adv., 4(15), pp. 3140–3191. DOI: https://doi.org/10.1039/D3MA00143A.

[7] Kuliiev, R. (2020). Mechanical properties of boron carbide (B4C).

[8] Jovanović, D., Zagorac, J.B., Matović, B., Zarubica, A.R. and Zagorac, D., 2020. Structural, electronic and mechanical properties of superhard B4C from first principles. Journal of Innovative Materials in Extreme Conditions, 1(1), pp.19-27.

[9] Kharat, W.S. and Sidhu, J.S., 2016. Development of epoxy based composites filled with boron carbide (B4C), tungsten disulphide (WS2) and evaluation of its mechanical properties. Int J Mech Eng Res, 6, pp.19-30.
[10] Abenojar, J., Martínez, M.A., Velasco, F., Pascual-Sánchez, V., Martín-Martínez, J.M. (2009). Effect of Boron Carbide Filler on the Curing and Mechanical Properties of an Epoxy Resin, The Journal of Adhesion, 85(4–5), pp. 216–238. DOI: https://doi.org/10.1080/00218460902881782.
[11] Rallini, M., Natali, M., Kenny, J.M., Torre, L. (2013). Effect of boron carbide nanoparticles on the fire reaction and fire resistance of carbon fiber/epoxy composites, Polymer, 54(19), pp. 5154–5165. DOI: https://doi.org/10.1016/j.polymer.2013.07.038.
[12] Abuali Galehdari, N., Kelkar, A.D. (2017). Effect of neutron radiation on the mechanical and thermophysical properties of nanoengineered polymer composites, J. Mater. Res., 32(2), pp. 426–434. DOI: https://doi.org/10.1557/jmr.2016.494.
[13] Revankar, S., Banapurmath, N.R., Sajjan, A.M., Nimbagal, V., Patil, A.Y., Venkatesh, R., Umarfarooq, M.A., Vadlamudi, C., Krishnappa, S. (2022). Epoxy-poly lactic acid blended composites reinforced with carbon fibres for engineering applications, Mat Express, 12(12), pp. 1502–1511. DOI: https://doi.org/10.1166/mex.2022.2303.
[14] Dileep, K., Srinath, A., Banapurmath, N.R., Umarfarooq, M.A., Sajjan, A.M. (2023). Mechanical and Fracture Characterization of Epoxy/PLA/Graphene/SiO2 Composites, Frattura Ed Integrità Strutturale, 17(64), pp. 229–239. DOI: https://doi.org/10.3221/IGF-ESIS.64.15.
[15] ASTM, D638-14:2014. Standard Test Method for Tensile Properties of Plastics, ASTM International, West Conshohocken, PA, USA 2014.
[16] ASTM D790, Standard test methods for flexural properties of unreinforced and reinforced plastics and electrical insulating materials, ASTM International, West Conshohocken, PA 2010.
[17] ASTM D4812-19e1, Standard Test Method for Unnotched Cantilever Beam Impact Resistance of Plastics. ASTM International: West Conshohocken, PA, USA, 2022.
[18] ASTM Standard D5045, Standard Test Methods for Plane Strain Fracture Toughness and Strain Energy Release Rate of Plastic Materials, ASTM International, West Conshohocken PA 1999, p. s2007
[19] Dileep, K., Umarfarooq, M.A., Srinath, A., Banapurmath, N.R., Sajjan, A.M. (2024). Impact of hybrid nanoparticle reinforcements on Mechanical properties of Epoxy-Polylactic Acid (PLA) Composites, Frattura Ed Integrità Strutturale, 18(70), pp. 91–104. DOI: https://doi.org/10.3221/IGF-ESIS.70.05.
[20] Varughese, J.J., M. S., S. (2024). Investigation on enhancement of filler dispersion and prediction of mechanical behavior of hexagonal boron nitride/epoxy nanocomposites through machine learning and deep learning models, Polymer Composites, 45(7), pp. 6287–6304. DOI: https://doi.org/10.1002/pc.28197.
[21] Umarfarooq, M.A., Choukimath, M., Banapurmath, N.R. (2024). Mechanical, Fracture, and Thermal Characterization of Post-Cured Hybrid Epoxy Nanocomposites Reinforced with Graphene Nanoplatelets and h-Boron Nitride, Fracture and Structural Integrity, 19(71), pp. 22–36. DOI: https://doi.org/10.3221/IGF-ESIS.71.03.
[22] Nimbagal, V., Banapurmath, N.R., Umarfarooq, M.A., Revankar, S., Sajjan, A.M., Soudagar, M.E.M., Shahapurkar, K., Alamir, M.A., Alarifi, I.M., Elfasakhany, A. (2023). Mechanical and fracture properties of carbon nano fibers/short carbon fiber epoxy composites, Polymer Composites, 44(7), pp. 3977–3989. DOI: https://doi.org/10.1002/pc.27371.
[23] B. Hiremath, G., R. Banapurmath, N., M. Sajjan, A., H. Ayachit, N., Badiger, N.M. (2025). Effect of Boron Nanoparticles on Epoxy Composites on Mechanical and Ionizing Radiation Protection Properties, Nuclear Technology, pp. 1–10. DOI: https://doi.org/10.1080/00295450.2025.2483055.
[24] Xie, Y., Kurita, H., Ishigami, R., Narita, F. (2020). Assessing the Flexural Properties of Epoxy Composites with Extremely Low Addition of Cellulose Nanofiber Content, Applied Sciences, 10(3), p. 1159. DOI: https://doi.org/10.3390/app10031159.